Fundamental Science-Based Simulation of Nuclear Waste Forms

Fuel Cycle Research & Development

Prepared for
U.S. Department of Energy
Fuel Cycle R&D Program
Ram Devanathan , Fei Gao, Xin Sun and Moe Khaleel
Pacific Northwest National Laboratory, Richland, WA 99352

September 2010
FCR&D-MDSM-2010-00168

Reviewed by:

Acting Director, Fuel Cycle Research and Development

Robert Price Date

Concurred by:

Director, AFCI Technical Integration Office

Phillip Finck Date

Approved by:

Deputy Assistant Secretary, Fuel Cycle Management

(AFCI Program Manager) Paul Lisowski Date

SUMMARY

This report presents a hierarchical multiscale modeling scheme based on two-way information exchange. To account for all essential phenomena in waste forms over geological time scales, the models have to span length scales from nanometer to kilometer and time scales from picoseconds to millennia. A single model cannot cover this wide range, and a multi-scale approach that integrates a number of different at-scale models is called for. The approach outlined here involves integration of quantum mechanical calculations, classical molecular dynamics simulations, kinetic Monte Carlo and phase field methods at the mesoscale, and continuum models. The ultimate aim is to provide science-based input in the form of constitutive equations to integrated performance and safety codes.

The atomistic component of this scheme is demonstrated in the promising waste form xenotime. Density functional theory calculations have yielded valuable information about defect formation energies. This data can be used to develop interatomic potentials for molecular dynamics simulations of radiation damage. Potentials developed in the present work show a good match for the equilibrium lattice constants, elastic constants and thermal expansion of xenotime.

In novel waste forms, such as xenotime, a considerable amount of data needed to validate the models is not available. Integration of multiscale modeling with experimental work is essential to generate missing data needed to validate the modeling scheme and the individual models. Density functional theory can also be used to fill knowledge gaps. Key challenges lie in the areas of uncertainty quantification, verification and validation, which must be performed at each level of the multiscale model and across scales. The approach used to exchange information between different levels must also be rigorously validated. The outlook for multiscale modeling of waste forms is quite promising.

CONTENTS

FIGURES

TABLES

ACRONYMS

AIMD	*Ab Initio* Molecular Dynamics
BKS	van Beest-Kramer-van Santen
DFT	Density Functional Theory
FCR&D	Fuel Cycle Research and Development
FMM	Force Matching Method
GGA	Generalized Gradient Approximation
GULP	General Utility Lattice Program
KMC	Kinetic Monte Carlo
MD	Molecular Dynamics
NEAMS	Nuclear Energy Advanced Modeling and Simulation
PNNL	Pacific Northwest National Laboratory
RDF	Radial Distribution Function
VASP	Vienna *Ab initio* Simulation Package
ZBL	Ziegler-Biersack-Littmark

FUEL CYCLE R&D PROGRAM
Fundamental Science-Based Simulation of Nuclear Waste Forms

1. INTRODUCTION

The aim of this report is to describe a fundamental science-based simulation method for studying atomic-level mechanisms that govern the radiation response of nuclear waste form materials and application of the method, in part, to a promising ceramic waste form.

The global expansion of nuclear power presents a solution to the problems arising from growing energy use worldwide, excessive dependence on energy from fossil fuels and the resulting adverse environmental impact, including the emission of green house gases [1]. At the same time, the use of nuclear power comes with concerns regarding nuclear proliferation and nuclear waste management [2]. It is essential to safely immobilize toxic nuclear waste, actinides in spent nuclear fuel, and plutonium from dismantled nuclear weapons using a science-based approach.

Nuclear waste has to be isolated from the biosphere over millennial time scales due to the toxicity of long-lived isotopes. Robust waste forms are an essential part of an integrated waste management strategy. Solid waste forms, which can be crystalline ceramics or glass matrices, represent the first line of defense against the transport of radionuclides. The efficacy of the waste form can be improved by using multiple engineered barriers and selecting a suitable repository [3]. Although the incorporation of high-level waste in borosilicate glass is preferred in several countries, this strategy presents challenges due to the metastablity of glass. Glass corrosion in humid atmospheres and microcracking may lead to radionuclide release. Crystalline ceramic waste forms need to be developed and evaluated as alternatives to glass, especially for the immobilization of Pu and minor actinides. It is well known that certain ceramics that have been advanced for waste form applications can eventually become amorphous when subjected to radiation with associated increase in the leaching rate of radionuclides. There is a pressing need to identify ceramics that can withstand radiation damage over millennia without losing their crystalline order by understanding radiation damage and annealing mechanisms starting with the fundamental atomic-level processes.

Extensive experimental studies [3] have provided mainly a phenomenological understanding of radiation effects in waste forms. Experimental studies are limited in their ability to study fundamental mechanisms, because the atomic-level processes that govern waste form performance are transient and occur on small length and time scales. At the same time, the laboratory experiment scale is many orders of magnitude shorter than the waste immobilization time scale and the repository length scale. It is also difficult in experiments to isolate individual mechanisms when multiple mechanisms occur together. Finally, the task of synthesis and characterization of waste forms with a high loading of actinides is hazardous, and there are only a limited number of experimental facilities where such work can be carried out safely. These limitations can be overcome by going beyond the conventional “heat and beat” approach by taking advantage of the ongoing explosive growth in computer processing speed and data storage, development of scalable computer codes, and advances in fundamental models and methods.

Fundamental science-based simulation can predict the behavior of waste forms under a variety of operating conditions, support what-if analysis under different accident scenarios, model experimentally inaccessible processes, and isolate individual mechanisms for study. Given the long span of length and time scale associated with waste immobilization, no single model can cover the whole range and one has to cleverly integrate multiple models from the atomistic to the repository scale. The results need to be validated at each scale using experimental study of chosen single effects and simulation results from finer

scales. The propagation of uncertainty across models and scales needs to be quantified to estimate the reliability of the predictions. This report provides a description of a multiscale modeling strategy centered at the level of first principles calculation and molecular dynamics (MD) simulation with particular emphasis on the development of interatomic potentials for modeling waste forms. The scope of the report includes a description of the modeling strategy, the need for development of reliable potentials, and analysis of results obtained from a recently developed potential for the waste form xenotime (YPO_4).

2. ATOMIC-LEVEL MODELS

2.1 Multiscale modeling

Accurate atomic-level simulations of radiation effects in ceramics serve as the foundation for science-based predictive modeling of waste forms. In order to accurately represent the interaction of nuclei and electrons in materials, one needs to perform simulations based on quantum mechanics. In recent years, density functional theory (DFT) has emerged as a valuable tool in materials science studies, especially in the area of defect chemistry [4]. DFT calculations are computationally intensive and are therefore limited to systems containing fewer than 1000 atoms. While DFT calculations offer excellent predictive capabilities, their utility is limited by the small system size which precludes the simulation of highly energetic processes and realistic systems that have surfaces, grain boundaries and dislocations. DFT-based *ab initio* molecular dynamics (AIMD) simulations are limited to very short time scales of the order of 10 ps. Waste form evolution involve phenomena that occur over multiple length and time scales. Realistic atomic level simulations that account for material inhomogeneity and access longer time and length scales require MD and kinetic Monte Carlo (KMC) calculations using reliable interatomic potentials. These methods, using the power of modern parallel computing architectures, can simulate systems containing millions to billions of atoms. The overall approach is illustrated in Fig. 1.

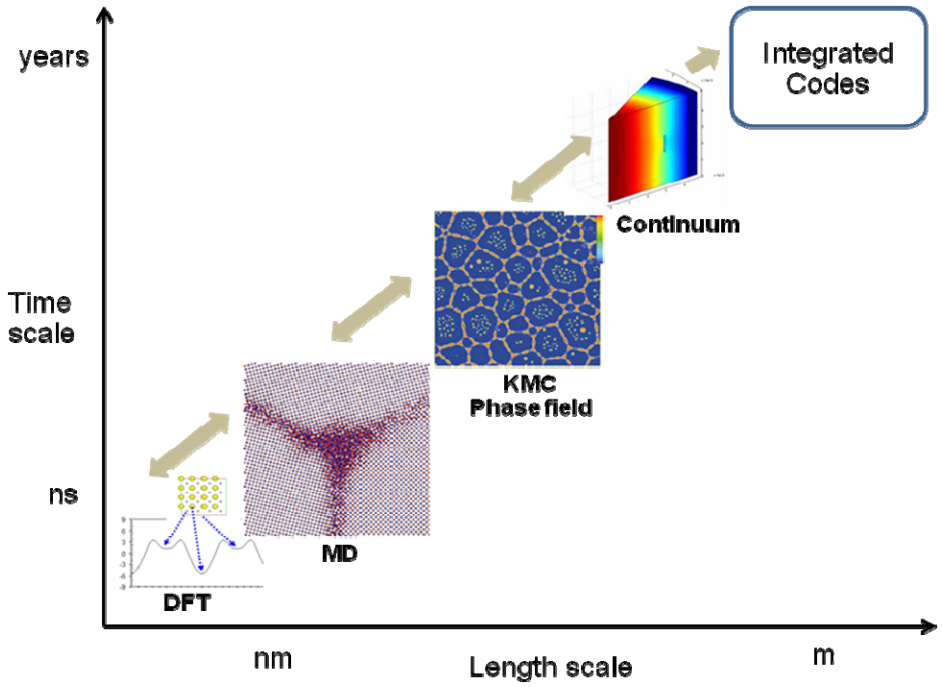

Figure 1. Hierarchical multiscale modeling scheme for waste forms.

2.2 Interatomic potentials

The interatomic potential is at the heart of MD simulations. Potentials describe the interaction between the atoms or ions in the system and determine the accuracy and speed of the simulation. Most of the interatomic potentials currently in use are obtained by fitting to a limited data set of experimentally determined properties of the equilibrium state but are used to simulate processes far from equilibrium. In other words, current interatomic potentials are not readily transferable to configurations significantly different from the ones to which they are fitted. The lack of reliable potentials often limits simulations to single component materials that have reasonably accurate potentials, for instance pure Fe as opposed to steel. Waste form materials are made of multiple elements and have complex structure and chemistry.

Rigorous efforts in fundamental theory and potential function development are needed to develop predictive simulation capabilities for waste form performance. This is especially important considering that the thermodynamic and kinetic properties calculated using MD serve to parameterize and validate simulations at the next coarser level in our scheme as shown in Fig. 1. In order to reduce the propagation of error up the modeling hierarchy, it is essential to improve the realism of interatomic potentials. At the same time, the process of fitting potentials also needs to be improved. At present, the fitting is accomplished by an arduous trial and error procedure that requires considerable manual effort. New functional forms that offer additional capabilities, such as reactivity and environment dependence, need to be developed. Such potentials would be valuable to study of waste form-water interactions.

The long-term goal of our efforts in this direction go beyond potential development for ceramics and development of new functional forms towards establishment of a systematic procedure for automated generation of transferable interatomic potentials from first principles and dynamic coupling of *ab initio* calculations with MD simulations. Our approach is based on the Force Matching Method (FMM) of Ercolessi and Adams [5]. The FMM uses a large amount of data obtained from DFT calculations of various configurations and AIMD simulations to fit the interatomic potential. Atomic forces are determined from first principles for a large number of configurations including geometries such as clusters, defects and simple model surfaces. The functional form and parameters of the potential are optimized to match the first principles forces by performing a minimization using a large parameter set. The method is not limited to currently used analytical forms, which is an advantage for the simulation of complex materials for which reliable potentials are not available at present.

The algorithm for potential generation using the FMM is schematically shown in Fig. 2. The procedure starts with an initial guess for the form of the potential. This first step requires a thorough understanding of the bonding characteristics in the material based on experimental data and DFT calculations of partial charges of ions, and charge transfer characteristics in the system. Here, one can go beyond conventionally used forms such as Buckingham, Morse, bond-order and Lennard-Jones. In addition to perfect crystal and metastable crystalline configurations, defect structures that are known from previous experiments and DFT calculations, and the amorphous state can be used as training sets for the force field. The next step is the determination of forces and energies from DFT. These forces along with experimentally determined lattice and elastic constants of various structures can be included in the fit. The data elements of the fit can be assigned various relative weights based on the confidence level associated with the data point. The potential can then be refined using a least-squares fit. Genetic algorithms are also being used increasingly in potential fitting. This scheme for the generation of the classical potentials can be used as a standalone module. It will involve providing the parameters of the interaction based on a number of configurations and then using this potential for large time- and length-scale classical MD simulations. The approach outlined here is highly relevant to simulations of defects, surfaces, grain size effects, and energetic recoil damage in novel ceramics for nuclear waste disposal, mineral water interfaces, and microbial surface interactions.

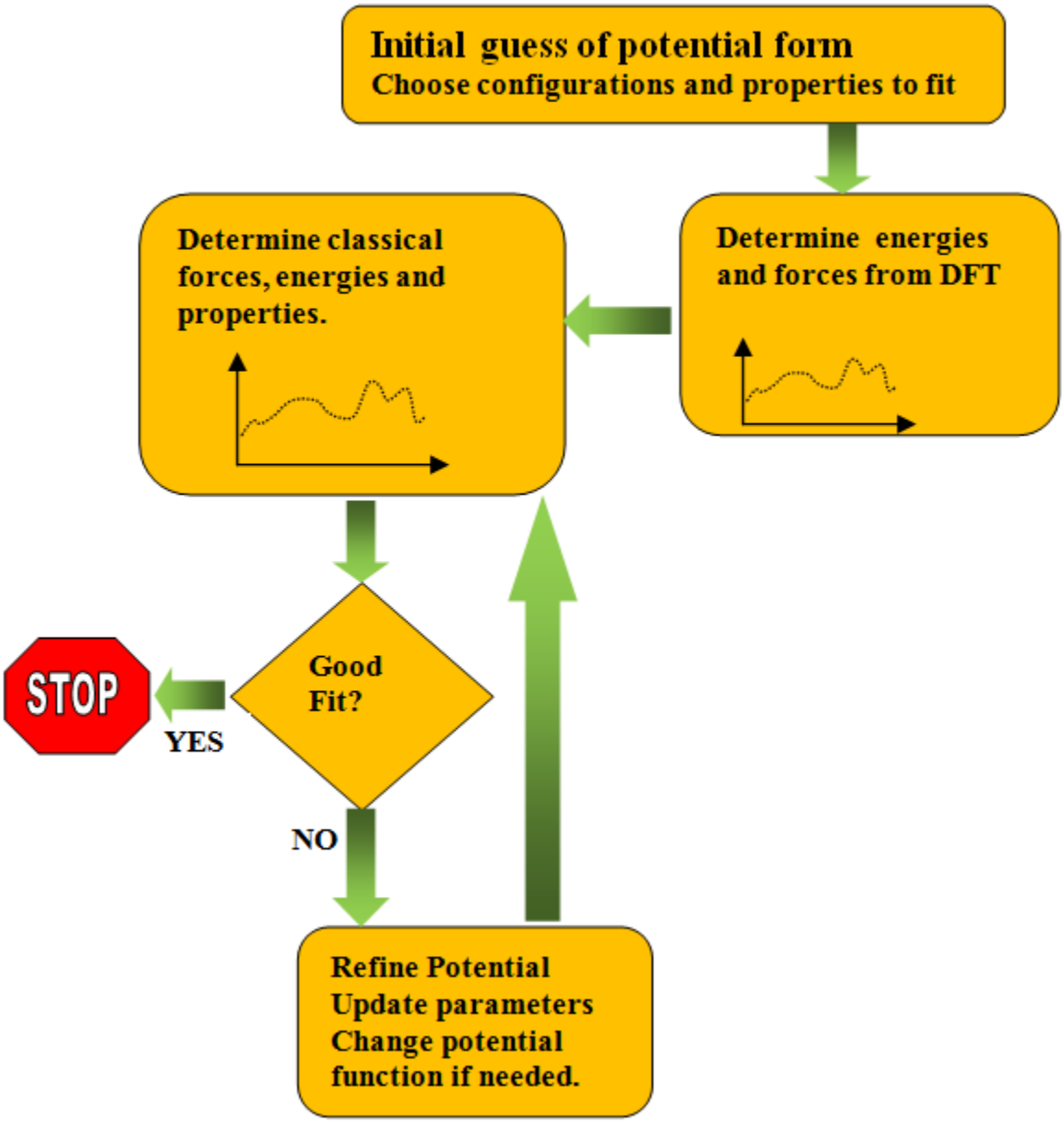

Figure 2. Algorithm for potential development.

A more challenging extension of the stand-alone module involves on-the-fly determination of interatomic potentials. This can be accomplished by loosely coupling a small quantum-mechanical simulation to a main classical MD simulation as shown in Fig. 3. The large MD simulation will pause if it encounters a configuration that is not well described by the interatomic potential and launch a small DFT-based simulation of the configuration of interest, which will refine the parameters of the interaction for the main simulation. Since the two simulations are only loosely coupled to each other, this affords an efficient implementation for thousands of processors. This scheme is relevant to problems where charge transfer processes are important and complex molecular environments and defect configurations are encountered.

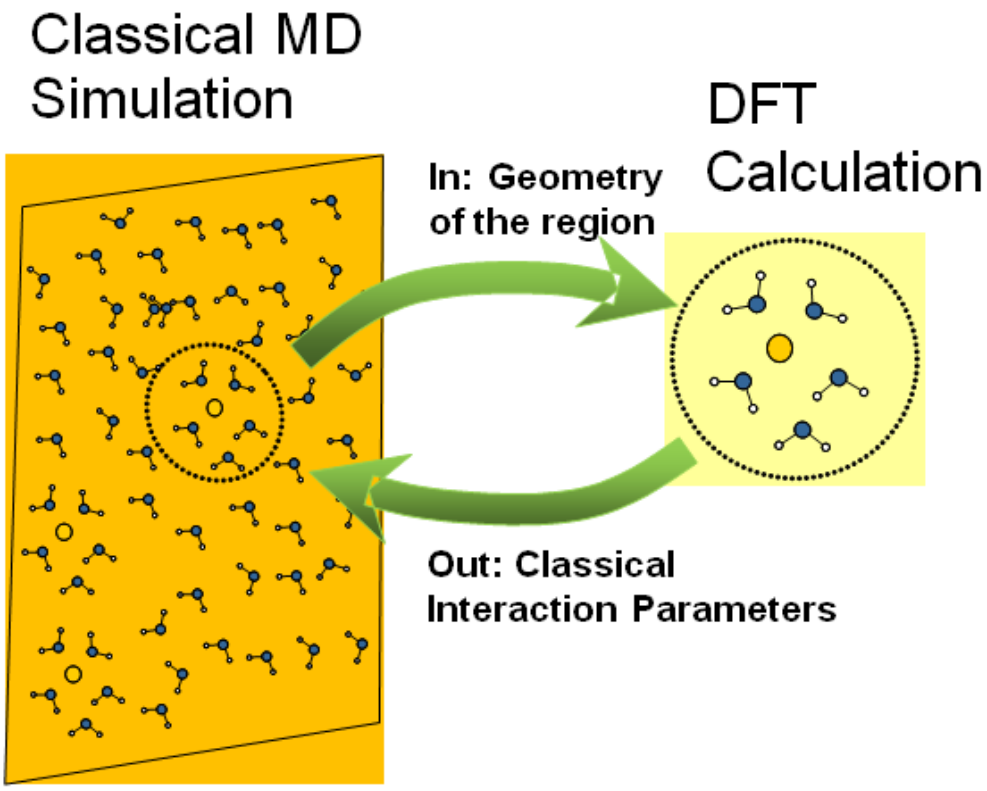

Figure 3. Scheme for coupling molecular dynamics simulations with density functional theory.

2.3 Ceramic potential functions

Ionic materials are often more challenging to simulate than metallic materials, because of the long range of the Coulombic interaction, partially covalent interactions and multiple charge states of ions (for instance Ce^{3+} and Ce^{4+}). Furthermore, actinide compounds are difficult to model because of electron correlations, relativistic effects and complex chemistry. The potential typically includes several components to represent the various types of interactions as discussed below.

The electrostatic interaction between ions i and j with charges q_i and q_j, respectively, separated by distance r_{ij} is given by the Coulomb potential as

$$V_C(r_{ij}) = \frac{q_i q_j}{4\pi\varepsilon_0 r_{ij}}, \quad (1)$$

where ε_0 is the permittivity of free space. q_i and q_j can be formal charges or partial charges determined based on first principles calculations. q_i and q_j can also be optimized by fitting to the properties of the ceramic.

Ionic polarizability can be included by using the shell model of Dick and Overhauser [6]. In this model an ion of charge $(Q+q)$ and mass M is represented as a core charge Q with mass M connected by a harmonic spring of spring constant k_{CS} to a massless shell of charge q as shown in Fig. 4. The Coulomb

interactions now include q_iq_j, Q_iQ_j, q_iQ_j and Q_iq_j terms. The spring interaction between the core and its shell in terms of the separation between their centers, Δr, is given by

$$V_S = \frac{k_{CS}(\Delta r)^2}{2}. \quad (2)$$

The ionic polarizability in terms of the shell charge, q, is given by

$$\alpha = \frac{q^2}{k_{CS}}. \quad (3)$$

The shell is typically applied only to anions, because the polarizability of cations is relatively smaller. Our practical experience suggests that MD simulations using shell model potentials require the use of time steps that are smaller by almost an order of magnitude relative to the time steps used with rigid ion models. Considerations of stability and computational cost generally preclude the use of shell models for large scale MD simulations and especially for simulations of energetic processes, such as recoils and thermal spikes.

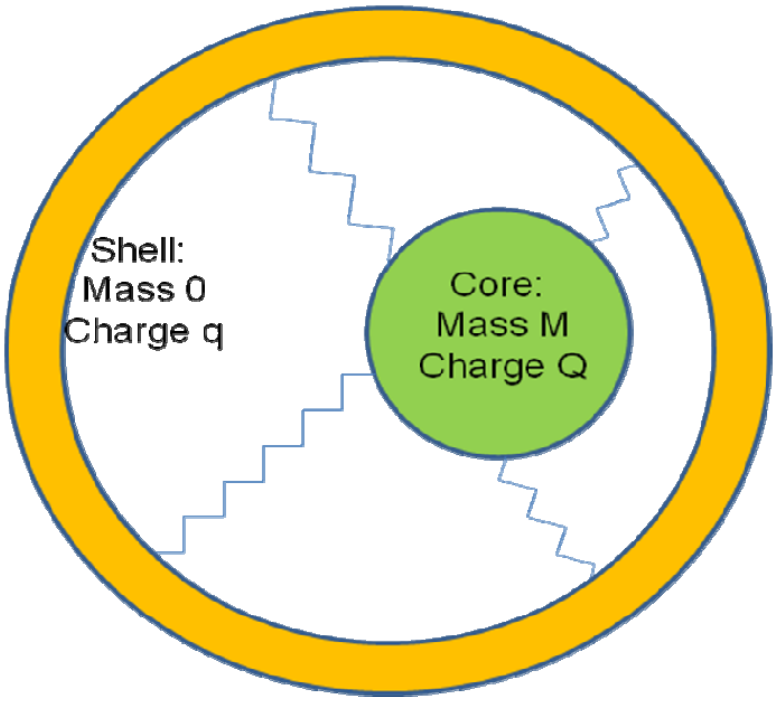

Figure 4. Shell model representation of ion of charge (Q+q) and mass M..

The short range repulsion and dispersion interaction are represented by the Buckingham potential as

$$V_B(r_{ij}) = A_{ij}e^{-\frac{r_{ij}}{\rho_{ij}}} - \frac{C_{ij}}{r_{ij}^6}. \quad (4)$$

If the system exhibits covalency, the potential can include the Morse term of the form

$$V_M(r_{ij}) = D_{ij}\left[e^{-2\beta_{ij}(r_{ij}-r_0)} - 2e^{-\beta_{ij}(r_{ij}-r_0)}\right]. \quad (5)$$

The parameter A_{ij}, ρ_{ij}, C_{ij}, D_{ij}, β_{ij} and r_0 are obtained by fitting to known properties of the material.

Bond length restraints can be imposed to maintain bond length r_{ij} close to a length r_1 using a harmonic spring with spring constant k_{ij} according to

$$V_d = k_{ij}(r_{ij} - r_1)^2. \quad (6)$$

Similarly, angle restraints can be imposed to maintain an angle, θ_{ijm}, close to angle θ_0 using a harmonic spring with spring constant k_{ijm} according to

$$V_a = k_{ijm}(\theta_{ijm} - \theta_0)^2. \quad (7)$$

In order to avoid unrealistic attraction due to the dominance of the dispersion term ($-\frac{C_{ij}}{r_{ij}^6}$) at short interionic distances that occur in radiation damage simulations, the pair potentials discussed above need to be joined smoothly using a spline function to the repulsive Ziegler-Biersack-Littmark (ZBL) potential [7]. The ZBL potential is a screened Coulombic repulsion between nuclei that is given by

$$\Phi(x) = 0.1818e^{-3.2x} + 0.5099e^{-0.9423x} + 0.2802e^{-0.4029x} + 0.02817e^{-0.2016x}, \quad (8)$$

where $x = \frac{r_{ij}(Z_i^{0.23} + Z_j^{0.23})}{0.8854a_0}$. (9)

a_0 is the Bohr radius (0.5292 Å) and Z_i and Z_j are the atomic numbers of ions i and j, respectively.

More complexity can be added to the interaction to account for reactivity. In developing potentials one has to make tradeoffs between accurately modeling a particular compound and transferability to an entire family of compounds, such as apatites, silicates or pyrochlores. Considerable work remains to be done to develop new functional forms for interatomic potentials in mixed ionic-covalent systems, reactive force fields that can account for charge redistribution during defect migration, stable potentials that can rigorously account for polarization, and a rigorous framework to verify and validate potentials. DFT calculations under conditions that are far from equilibrium are needed to examine the range of validity of interatomic potentials. This will help overcome the limitations of conventional potential development that uses equilibrium properties to fit potentials that are then used to simulate phenomena far from equilibrium and thus outside the range of validity of the potentials.

2.4 Links to higher scales

Once a reliable interatomic potential is obtained, one can simulate the primary damage state and study structural changes brought about by radiation using the MD method. The simulated results need to be validated against experimental data, such as thermal conductivity and volume expansion. The output of MD studies of waste forms can include the following:

- Nanoscale spatial distribution of defects
- Densities of defects, such as vacancies and interstitials
- Change in density of the material upon irradiation
- Energetics of aggregation of point defects into clusters and defect-impurity complexes
- Migration energies of defects and defect clusters and diffusion mechanisms
- Interaction of point defects and defect clusters with interfaces and extended defects
- Nucleation of voids, cracks and dislocation loops
- Changes in thermal conductivity due to defects, voids and cracks

X-ray diffraction, high-resolution transmission electron microscopy, high-resolution Rutherford backscattering spectroscopy and helium ion microscopy along with mechanical property measurements can provide validation for the simulation results at this scale.

The output of MD simulations can be used to develop continuum thermo-chemical models of point defect concentrations and ionic diffusivity in waste forms under repository conditions, as well as an assessment of rate coefficients to be used in mesoscale models of waste form microstructure evolution. Microstructural evolution under irradiation has unique features that are not encountered during conventional materials processing. Radiation damage accumulation leads to gradual swelling of the lattice and increases the probability of leaching of actinides. The interaction of radiation-damaged waste form microstructures with water over geologic time scales is a challenge for multiscale modeling. The elevated temperature and temperature gradients present in these materials can enhance diffusion and influence the kinetics of many defect processes.

The thermodynamic parameters generated using MD simulations can be used as input for higher-scale models. Two mesoscale models of microstructural evolution, namely phase-field and kinetic Monte Carlo, are being considered as possible links between the MD scale and the continuum scale to understand and predict waste form behavior. These mesoscale models require accurate thermodynamic and kinetic parameters for defects and fission products, such as the generation rate of point defects, defect mobilities and their reactions, defect energetics, mechanical properties of different phases, interfacial energies, and interface mobility. Since such information does not exist in a form that is readily used by mesoscale models, atomistic simulations can be employed to generate such a database.

2.4.1 Kinetic Monte Carlo Model

The Potts kinetic Monte Carlo (KMC) is a statistical-mechanical model that populates a lattice with an ensemble of discrete particles to represent and evolve the microstructure. The particles represent a discrete quantity of material that is much larger than an atom. The evolution of the particles is used to simulate microstructural changes. The Potts KMC used for mesoscale simulations is distinct from atomistic KMC, which simulates processes at the atomic level. The Potts KMC method has the advantage of being simple and intuitive to visualize, while still being a rigorous method that can incorporate all the thermodynamic, kinetic and topological characteristics to simulate complex processes. This method is readily extendable from two to three dimensions and can simulate the underlying physics of many materials evolution processes based on the statistical-mechanical nature of the model. The microstructure is represented as an ensemble of particles that occupy a regular lattice. . Lattices can be triangular, square, cubic or other geometries. The most commonly used geometries are square and cubic lattices. It is possible to perform KMC with non-lattice based methods. However, the vast majority of KMC models use regular lattices.

The KMC particles can be considered to be a discrete amount of material that is much larger than an atom; thus all atomistic characteristics are aggregated into discrete extensive thermodynamic quantities such as mass and energy for each particle. The total system energy is quite naturally the sum of the energies of each particle. Particle energies can be categorized as interfacial or bulk. Interfacial energies are associated with particles that are on an interface such as a grain boundary, pore surface or precipitate interface. The form of the energy is quite versatile and can be matched to the characteristics of real materials. The interfacial and bulk energies can be functions of the microstructure or materials, so that as the system evolves due to changing chemistry or accumulation of radiation damage, the particle energies can reflect the current thermodynamic state. This ability to easily tailor particle energies makes KMC models highly versatile and widely applicable to many materials evolution processes. KMC models can provide a detailed picture of the microstructure and its evolution in response to a given set of starting conditions and applied conditions. The microstructure evolves in response to local conditions that may also be changing with time and position. The adaptation of KMC models to the specific processes relevant to waste forms is a crucial need. The previous use of KMC models [8, 9] to correctly simulate various processes, such as grain growth, sintering and recrystallization, is cause for optimism regarding the suitability of KMC methods for modeling nuclear waste forms.

2.4.2 Phase Field Model

The phase-field model is a deterministic, continuum, thermodynamic model that describes the microstructure and its evolution in terms of evolving continuum phase fields that can be grain orientations, composition, phases or other microstructural and compositional descriptors. While the phase-fields themselves are continuum quantities, solving their field equations on some predefined grid – typically square in 2D and cubic in 3D simulates their evolution. The size of the grid is such that the distance between solution points is much larger than typical interatomic distance but sufficiently small to resolve microstructural features such are grain boundaries.

The phase field method is considered a powerful mesoscale modeling method and is widely used to model the kinetics of microstructural evolution in materials. The energy of the system is defined by a free energy functional which is a function of the phase fields and their gradients. An advantage of the phase-field method for waste form modeling is that various defects, voids and microstructural features with moving boundaries can be easily treated. In addition, the thermodynamic driving force for microstructure evolution can be incorporated based on input from experimental databases and lower length scale models. These include bulk chemical free energy, interfacial/surface energy, elastic strain energy, and electrostatic energy. Traditionally, phase field models have simulated quasi-equilibrium phenomena. In order to reliably model the highly non-equilibrium nature of radiation effects in nuclear materials [10] one has to explicitly include the energetics of processes such as defect production by irradiation, and this is a major challenge.

Existing phase field models are mainly two-dimensional. The model must be extended to three dimensions to realistically model waste forms. Another limitation of phase field models at present is that they provide mainly qualitative information about microstructural changes under irradiation. As mentioned above, quantitative modeling requires accurate thermodynamic and kinetic input from lower scales, such as first principles calculations and classical MD simulations. The required input includes the size and spatial distribution of defect clusters, relationship between defect concentration and chemical free energy, point defect and defect cluster mobilities and binding energies, defect interaction energies, and realistic models of grain structure. Quantitative modeling is essential for uncertainty quantification, verification and validation. Validated information from phase field models can be passed on as constitutive equations to higher-level continuum models as illustrated in Fig. 1.

The next section discusses atomistic models applied to xenotime, which is a promising nuclear waste form.

3. MULTISCALE MODELING OF XENOTIME

3.1 Xenotime waste form

Xenotime (YPO_4) is an orthophosphate that occurs in nature with significant concentrations of U and Th. It can be used an alternative to monazite or zircon in geochronology studies. Given that both zircon, monazite and xenotime have shown stability in nature over millennial time scales while retaining from ppm levels to a few percent of actinides, they are considered candidate ceramic waste forms. In this regard, the radiation response of zircon ($ZrSiO_4$) has been extensively studied by experiment [11] and simulation [12]. These studies have shown that zircon is easily amorphized by heavy ion irradiation. However, in general, phosphates are considered to be more radiation resistant than silicates and the reasons for the radiation resistance are not well-understood. This significant difference in radiation response of zircon and xenotime is surprising given that they have the same structure and are isoelectronic. The difference in cation charge states (Zr^{4+} vs. Y^{3+} and Si^{4+} vs. P^{5+}) and differences between silicate and phosphate networks could be key factors underlying the radiation response. However, these issues have not been explored in detail to date, and the mechanisms governing the relative radiation tolerance of these waste forms is not well understood. Thus, by simulating radiation damage in xenotime, one can not only gain insights into the fundamental processes that underlie the radiation response of a promising waste form but also understand the role of chemical bonding differences in determining radiation response.

The structure of xenotime is shown in Fig. 5. The crystal structure is body-centered tetragonal (space group I41/amd) with four YPO_4 formula units per unit cell [13]. The *c* lattice parameter (vertical direction) is shorter than the *a* lattice parameter (horizontal direction in Fig. 5). The arrangement of O is such that the structure consists of edge sharing PO_4 tetrahedra and YO_8 dodecahedra. Each P is coordinated by 4 O at a bond distance of 1.54 Å, while each Y is coordinated by 4 O at 2.31 Å and 4 O at 2.38 Å as shown by the body centered atom in Fig. 1. Each O is bonded to two Y and one P. The P atoms are not joined by common O neighbors.

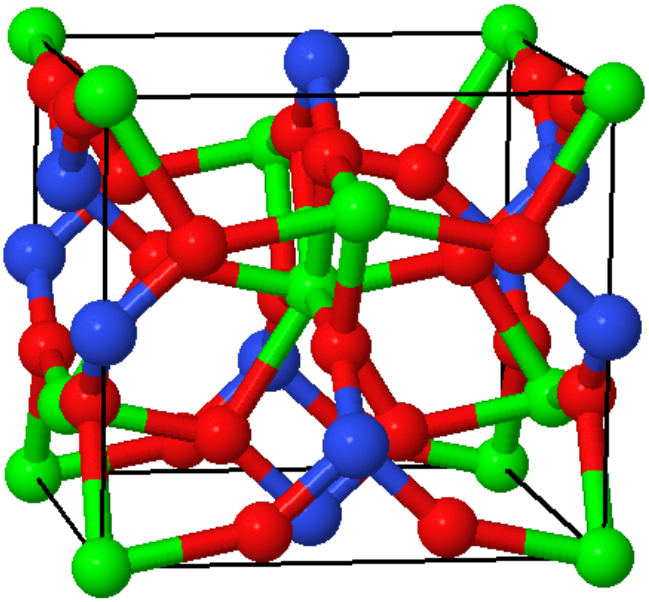

Figure 5. The crystal structure of YPO_4. Y, P and O atoms are shown in green, blue and red, respectively.

3.2 DFT calculations of defects in xenotime

DFT calculations of the formation energy of defects in xenotime were performed with the Vienna *ab initio* simulation package (VASP) to develop a database of defect properties for use in the proposed multiscale modeling scheme [14]. The interaction between ions and electrons was described using the projector augmented wave method [15], and the exchange correlation functional was determined within the generalized gradient approximation (GGA) parameterized by Perdew and Wang [16]. Accurate convergence studies were performed to get an absolute convergence of a few meV for every electronic level. The calculations used plane wave basis set for valence electrons with a cutoff energy of 500 eV.

The defect calculations were based on a 2x2x2 supercell, in which the perfect crystal contained 192 atoms. The vacancy defect formation energies were calculated using the equation

$$E_F^{VacX} = E^{VacX} - E_{tot} + E_X , \tag{10}$$

where E^{VacX} is the total energy of the supercell containing one X vacancy, E_{tot} is the total energy of the ideal structure, and E_X is the energy per X atom in its bulk phase. The formation energies for interstitial defects were calculated using the expression

$$E_F^{IntX} = E^{IntX} - E_{tot} - E_X , \tag{11}$$

where E^{IntX} is the total energy of the relaxed supercell containing one X interstitial. The antisite formation energies were calculated using the equations

$$E_F^{AS_{pair}} = E^{AS_{pair}} - E_{tot} \tag{12}$$

and

$$E_F^{X_Y} = E^{X_Y} - E_{tot} - E_X + E_Y \tag{13}$$

Here, $E^{AS_{pair}}$ and E^{X_Y} are the total energy of the supercell with antisite pair (exchange of the neighboring Y and P atoms) and X_Y antisite defects (an X atom located on a Y site), respectively. For Frenkel pairs, relaxation of the structures resulted in correlated recombination of the interstitial with the vacancy at its original site. The Frenkel-pair defect formation energy is defined by the energy difference between the optimized perfect structure and the relaxed defect structure. Similar methods have been previously used to calculate defect formation energies in stannate pyrochlores [17]. Some of the defects studied are illustrated in Fig. 6. Table I provides a list of defect energies studied. This can be used to validate xenotime potentials in the future and also provide thermodynamic input for mesoscale models.

3.3 Xenotime interatomic potential

There is limited information on simulations of xenotime in the literature. Experimental studies have reported lattice constants, elastic constants and thermal expansion data. Previously, Rabone and de Leeuw [18] had developed a transferable shell-model potential for phosphates that is applicable to apatites and rare earth phosphates. This potential is not suitable for dynamic simulations of energetic processes, because of the shell model.

Table I. Defect formation energies calculated using DFT

Defects	Defect formation energy (eV)
Vacancies	
Y_{vac}	15.09
P_{vac}	17.94
O_{vac}	14.29
Antisite defects	
Antisite pair	12.66
Y_P	6.22
P_Y	10.06
Interstitials	
Y_{int1}	11.39
Y-Y splitting toward int1	11.55
Y_{int2}	7.75
P_{int1}	9.24
P-P splitting toward int1	10.53
O_{int1}	3.39
O-O splitting toward int1	2.53
O_{int2}	4.36
O-O splitting toward int2	2.53
Frenkel pairs	
$Y_{vac}+Y_{int1}$	48.68
$Y_{vac}+Y_{int2}$	28.18
$P_{vac}+P_{int1}$	19.56
$O_{vac}+O_{int1}$	11.42
$O_{vac}+O_{int2}$	12.01

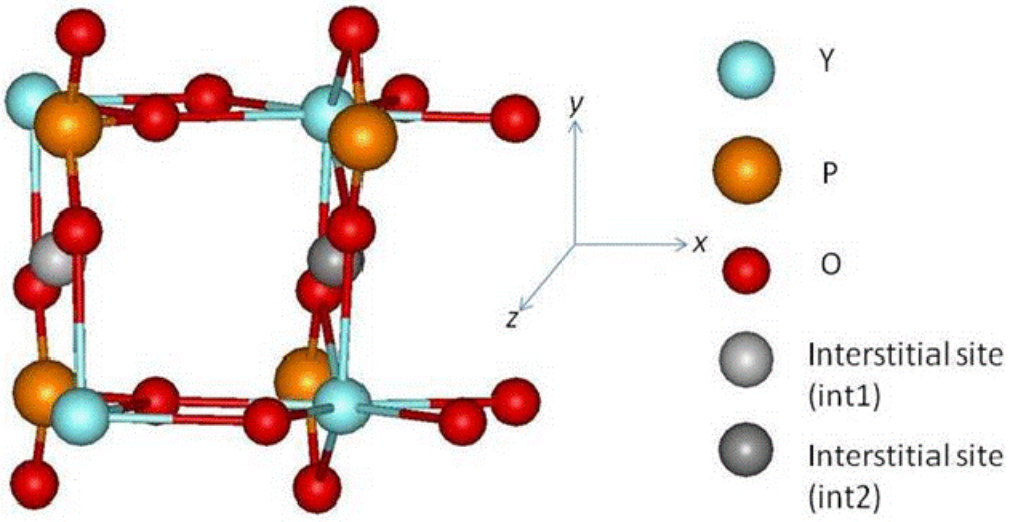

Figure 6. Schematic view of some of the defects in YPO_4 that were studied using DFT.

DFT calculations of the perfect crystal configuration and point defects discussed in the previous section represent a big step forward but are not sufficiently comprehensive at this point to fully guide potential development. Therefore, YPO_4, potentials were developed based on fitting to available experimental data. Based on past experience with interatomic potential fitting for zircon and urania, a combination of Coulombic, Buckingham and Morse potential forms were chosen for YPO_4. In future, the potentials will be refined and validated using the growing DFT database. In the first fitting iteration, a rigid ion model was chosen with charges of -1.2, 1.8 and 3.0 for O, Y and P, respectively. In addition to the Coulombic interaction (Eq. 1), the short-range Buckingham interaction (Eq. 4) was included. The Buckingham parameters for the O-O interaction were chosen to be the same as those of the well known BKS potential [19], which has been successfully used to model silicates. Least-squares fitting to lattice and elastic constants was performed using the GULP computer code [20] in the constant pressure ensemble at 0 K with a relaxed fitting procedure. The parameters of the potential are given in Table II.

Table II. Parameters of the YPO_4 potential Xen01

Parameter	$\mathbf{Y^{1.8}\text{-}O^{-1.2}}$	$\mathbf{P^{3.0}\text{-}O^{-1.2}}$	$\mathbf{O^{-1.2}\text{-}O^{-1.2}}$
A_{ij} (eV)	21788.1178	50.0043	1388.773
ρ_{ij} (Å)	0.3174	0.8833	0.3623
C_{ij} (eV.Å^6)	2788.9071	0.0	175.0

The suitability of potential Xen01 to model YPO_4 was evaluated by examining its ability to reproduce known elastic constants and lattice constants [18, 21] in static calculations by minimizing the energy of the system using the Newton Raphson optimizer with Broyden-Fletcher-Goldfarb-Shanno updating of the Hessian matrix [22] using the GULP code [20]. The results are shown in Table III. Although the fit obtained appears to be reasonable, the YPO_4 structure was unstable in MD simulations using the DL_POLY code [23] at finite temperature. The low value of the elastic modulus C_{66} could be a contributing factor for the instability.

Table III. Lattice and elastic constants of YPO_4 from the potential Xen01

Property	**Potential Xen01**	**Experiment [21]**
Lattice constant *a* (Å)	6.852	6.883
Lattice constant *c* (Å)	6.092	6.021
C_{11} (GPa)	158	220
C_{12} (GPa)	20	55
C_{13} (GPa)	76	86
C_{33} (GPa)	311	332
C_{44} (GPa)	62	65
C_{66} (GPa)	5	17

In a subsequent fit, the idea of keeping the O-O interaction the same as the BKS potential was abandoned. In addition to the Coulombic interaction (Eq. 1) and short-range Buckingham interaction (Eq. 4), a Morse interaction for P-O was introduced to maintain optimum P-O separation. The charges were varied to achieve a good fit to lattice constants and elastic constants. The optimized rigid ion model has charges of -0.9, 1.35 and 2.25 for O, Y and P, respectively. The parameters of this potential are given in Table IV.

Table IV. Parameters of the YPO_4 potential Xen02

Parameter	**$Y^{1.35}$-$O^{-0.9}$**	**$P^{2.25}$-$O^{-0.9}$**	**$O^{-0.9}$-$O^{-0.9}$**
A_{ij} (eV)	250989.0940	116.9199	423.3573
ρ_{ij} (Å)	0.1702	0.1388	0.3877
C_{ij} (eV.Å^6)	121.8523	0.0	0.0
D_{ij} (eV)	0.0	8.296	0.0
β_{ij} (Å^{-1})	0.0	14.444	0.0
r_0 (Å)	0.0	1.528	0.0

Table V. Lattice and elastic constants of YPO_4 from the potential Xen02

Property	**Potential Xen02**	**Experiment [21]**
Lattice constant *a* (Å)	6.885	6.883
Lattice constant *c* (Å)	6.043	6.021
C_{11} (GPa)	221	220
C_{12} (GPa)	41	55
C_{13} (GPa)	88	86
C_{33} (GPa)	331	332
C_{44} (GPa)	71	65
C_{66} (GPa)	30	17

The fit of potential Xen02 to the lattice constants and elastic constants of YPO_4 is shown in Table V. Although the potential Xen02 provides a much improved fit to experimentally-obtained equilibrium properties compared to Xen01, the structure was found to be unstable in MD simulations upon heating to 500 K. These results show that static structure optimization is not sufficient and the stability of the crystal has to be tested in dynamic simulations at elevated temperature and by comparing the energy of the perfect crystal to that of a disordered crystal.

In an effort to stabilize the xenotime structure, a new potential model was tested. In this model, Xen03, the PO_4 tetrahedra were kept intact through bond and angle restraints [18]. The system was made up of $Y^{+2.22}$ and $PO_4^{-2.22}$ ions. Buckingham-type short range interactions were implemented for Y-O and O-O. The parameters of the potential are given in Table VI. These potentials were developed in collaboration with Prashant Selvaratnam and Ian Farnan at University of Cambridge (UK).

The fit of potential Xen03 to the lattice constants and elastic constants of YPO_4 is shown in Table VII. The lattice constants are fitted almost perfectly, and all the elastic constants with the exception of C_{12} are fitted very well. Attempts to fit C_{12} accurately resulted in poor fits to C_{66} and C_{44}. The inability to fit all the elastic constants very well is due to the limitations of the presently used simple functional form and the neglect of polarizability for the sake of computational convenience. In addition, the bond lengths given by this potential are as follows with the experimental data in brackets.

Y-O bonds: 4 at 2.31 (2.31 Å) and 4 at 2.38 (2.38 Å)

P-O bonds: 4 at 1.54 (1.54 Å)

O-O bonds: 1 at 2.39 (2.41 Å), 2 at 2.58 (2.57 Å), 1 at 2.78 (2.80 Å) and 4 at 2.96 (2.96 Å).

The xenotime structure was found to be stable in MD simulations up to 2000 K.

Table VI. Parameters of the YPO_4 potential Xen03

Parameter	$\mathbf{Y^{2.22}\text{-}O^{-0.905}}$	$\mathbf{P^{1.40}\text{-}O^{-0.905}}$	$\mathbf{O^{-0.905}\text{-}O^{-0.905}}$
A_{ij} (eV)	6964.2003	116.9199	1956.9708
ρ_{ij} (Å)	0.2342	0.1388	0.2864
C_{ij} (eV.Å^6)	0.0967	0.0	0.1018
D_{ij} (eV)	0.0	7.7934	0.0
β_{ij} (Å^{-1})	0.0	5.2514	0.0
r_0 (Å)	0.0	1.5444	0.0
k_{OPO} (eV/rad^2)		1.32	
θ_{OPO} (deg)		109.47	

Table VII. Lattice and elastic constants of YPO_4 from the potential Xen03

Property	**Potential Xen01**	**Experiment [21]**
Lattice constant *a* (Å)	6.895	6.883
Lattice constant *c* (Å)	6.029	6.021
C_{11} (GPa)	220	220
C_{12} (GPa)	28	55
C_{13} (GPa)	93	86
C_{33} (GPa)	337	332
C_{44} (GPa)	65	65
C_{66} (GPa)	17	17

3.4 Simulations of thermal expansion of xenotime

We have performed classical MD simulations of xenotime at various temperatures using the Xen03 potential and the DLPOLY code [23]. The simulation cell contained 3000 ions (5x5x5 unit cells) with periodic boundaries. The system was initially equilibrated at 300 K and zero external pressure for 10 ps with Berendsen's isothermal isobaric ensemble [24]. Subsequently, the system was equilibrated at temperatures between 300 and 2100 K for 2.5 ps with the isothermal isobaric ensemble, and a time step of 1 fs was employed. The production run at each temperature was 2.5 ps. Energy conservation was better than 1 in 10^4 at all temperatures studied. The system remained in the xenotime crystal structure. The variation of the enthalpy per atom and density with temperature are shown in Fig. 7. The coefficient of linear thermal expansion calculated from MD simulations is 8×10^{-6} K^{-1}, which is in reasonable agreement with the experimental value of 6×10^{-6} K^{-1}.

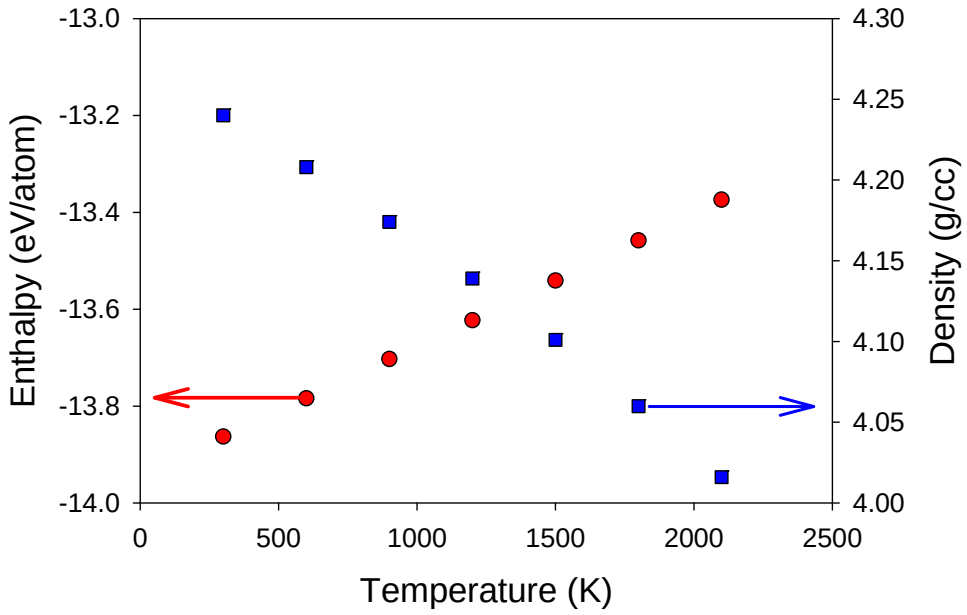

Figure 7. Changes in enthalpy (red circle; left ordinate) and density (blue square; right ordinate) of xenotime with temperature from MD simulation.

The crystal of xenotime was heated to 4000 K and equilibrated with the isothermal isobaric ensemble for 20 ps. Melting occurred as determined by the radial distribution function (RDF) and diffusion coefficients of ions. The molten system was equilibrated at 4000 K for a further 100 ps and quenched to 300 K at the rate of 10^{14} K/s. This quench rate is orders of magnitude faster than the rates that can be achieved in experiment, but is used because it is not currently computationally feasible to perform ms-time scale MD simulations to achieve the low quench rates characteristic of experiments. The density of the resulting amorphous phosphate was 3.26 g/cc, which represents a decrease of 23.1% from the perfect xenotime crystal value of 4.24 at 300 K. We were unable to obtain experimental data to validate the potential based on the value of density change upon amorphization. In the future, detailed melting studies at crystal-amorphous interfaces will be carried out to validate the potential model and to refine it further.

The RDF of Y-O, P-O and O-O pairs in crystalline xenotime at 300 K is shown in Fig. 8 (a) alongside the corresponding RDF in amorphous YPO_4 in Fig. 8(b). There is evidence of long-range structure in the crystal, but this disappears beyond 5.5 Å in the amorphous material. The Y-O distance is also shorter in the amorphous material compared to that in the crystal. These trends are reflected in the changes in the number of oxygen neighbors of Y, P and O as a function of distance plotted in Fig. 9 (a) for crystalline YPO_4 and Fig. 9(b) for amorphous YPO_4. The steps in the plot for the crystal show the existence of structure. These are missing beyond the first neighbor separation in amorphous YPO_4. The destruction of long-range order upon amorphization can also be clearly seen in Fig. 10, which presents P-P, Y-P and Y-Y RDF plots in the crystal and amorphous material. The P-P and Y-P distributions are identical in the crystal but differ in the amorphous material. The ions have moved apart, which is an indication of the considerable volume expansion that occurs with amorphization.

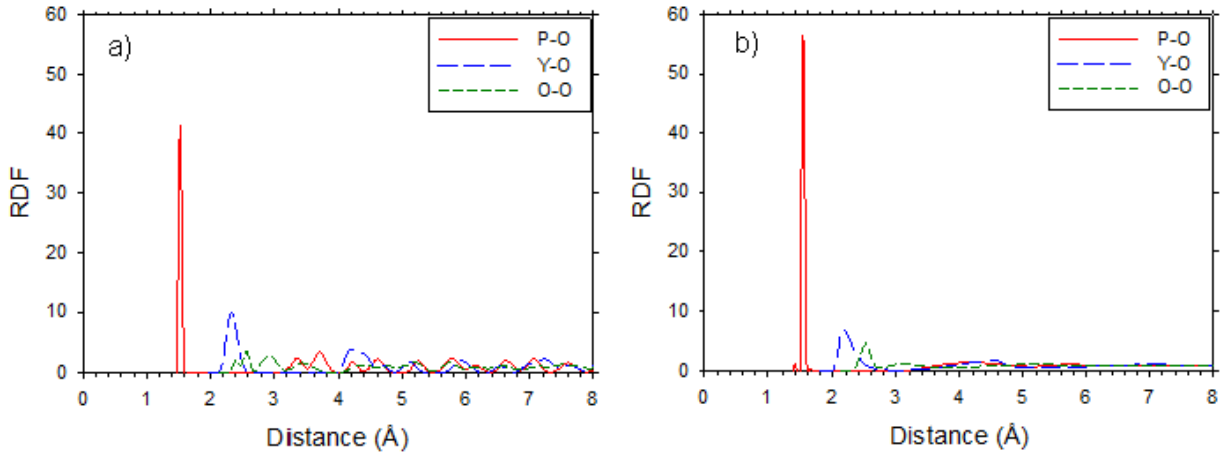

Figure 8. Cation-anion RDF plots at 300 K in a) crystalline YPO_4 and b) amorphous YPO_4.

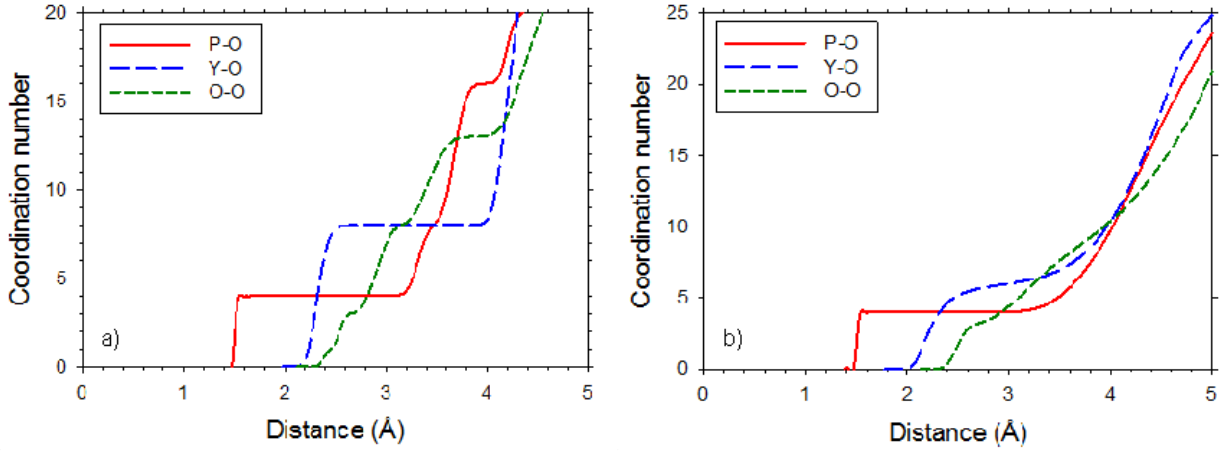

Figure 9. Number of O neighbors of P, Y and O vs. distance in a) crystalline and b) amorphous YPO_4.

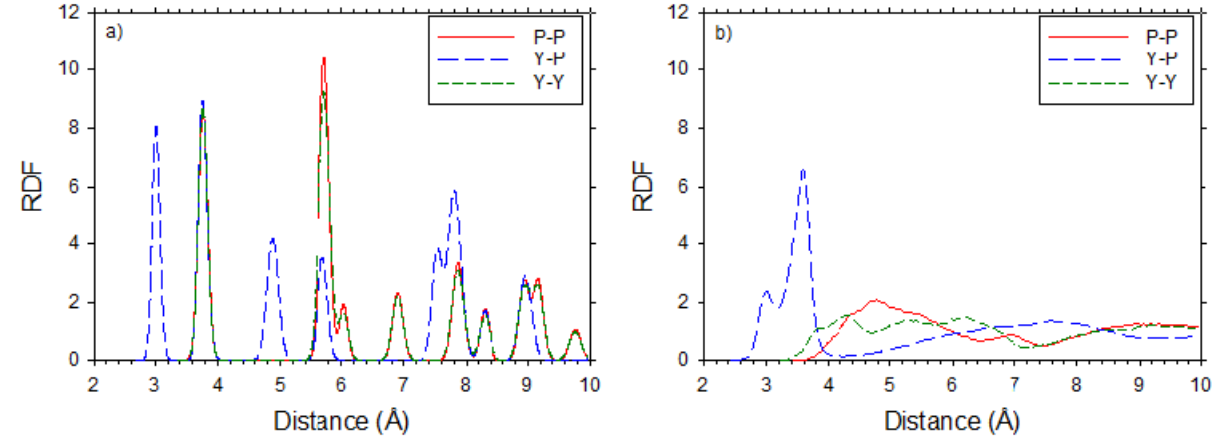

Figure 10. Cation-cation RDF plots at 300 K in a) crystalline and b) amorphous YPO_4.

4. SUMMARY AND OUTLOOK

The MD simulation cells considered in this study measure about 35 Å x 35 Å x 30 Å. Certainly, much larger systems need to be simulated to examine the effects of energetic recoil damage on the structure and properties of waste forms. Following further validation and refinement of the currently used interatomic potential using extensive DFT data and experimental observations, large scale simulations of recoil events can be carried out using MD. By initiating the recoils inside the material and using periodic boundaries one can study the primary damage state, defect generation, defect clustering, and the recombination volume of defects. Grain boundaries, interfaces and extended defects can be included in the simulation, and defects observed in the primary damage state can be systematically introduced separately near the grain interior and the grain boundary. Such a multiscale approach is already being pursued elsewhere for nuclear fuels [25].

DFT simulations or classical MD can be extended to determine the migration barriers for defects such as vacancies and interstitials. Since the barriers will depend on the presence of point and extended defects in the vicinity of the migrating defect, DFT calculations can be used to calculate defect formation energies and defect migration barriers mainly in small, near-perfect systems. In order to calculate energy barriers and binding energies in realistic systems that have grain boundaries and interfaces, classical MD can be used to develop a large database of defect properties. In developing such a database, a weight factor needs to be attached to each datum based on the uncertainty in the value.

The work presented in the previous section is a step forward towards achieving the goal of multiscale modeling of waste forms. Defect formation energies were determined using DFT calculations, and potential models were evaluated and refined. Much work remains to be done in integrating this atomistic level to the mesoscale represented by KMC and phase field models and onward to the continuum scale. Given the growing processing power of computers and the emergence of new hybrid computational architectures and robust parallel codes, the prospects for science-based simulation of waste forms are quite bright.

REFERENCES

1. W. C. Sailor, D. Bodansky, C. Braun, S. Fetter and R. van der Zwaan, *Science* **288(5469)**, 1177 (2000).
2. R. C. Ewing, *MRS Bulletin* **33**, 338 (2008).
3. R. C. Ewing, *Proc. Natl. Acad. Sci*., **96**, 3432 (1999).
4. A. E. Mattsson, P. A. Schultz, M. P Desjarlais, T. R Mattsson and K. Leung, *Modell. Simul. Mater. Sci. Eng*. **13**, R1-R31 (2005)
5. F. Ercolessi and J. B. Adams, *Europhys. Lett.* **26**, 583 (1994).
6. B. G. Dick and A. W. Overhauser, *Phys. Rev*. **112**, 90 (1958).
7. J. F. Ziegler, J. P. Biersack, and U. Littmark, *The Stopping and Range of Ions in Matter*, (Pergamon Press, New York, 1985).
8. E. A. Holm, M. A. Miodownik and A. D. Rollett, *Acta Mater*. **51**, 2701 (2003).
9. V. Tikare, M. Miodownik, E. A. Holm, *J. Am. Ceram. Soc.* **84**, 1379 (2001).
10. S. Y. Hu, Y. L. Li, X. Sun, F. Gao, R. Devanathan, C. H. Henager Jr. and M. Khaleel, *Intl. J. Mater. Res.* **101**, 515 (2010)
11. I. Farnan, H. Cho and W. J. Weber, *Nature* **445**, 190 (2007).
12. R. Devanathan, L. R. Corrales, W. J. Weber, A. Chartier and C. Meis, *Mol. Sim*. **32**, 1069 (2006).
13. Y. Ni, J. M. Hughes and A. M. Mariano, *Am. Mineralog*. **80**, 21 (1995).
14. G. Kresse and J. Furthmüller, *Phys. Rev. B* **54**, 11169 (1996).
15. G. Kresse and D. Joubert, *Phys. Rev. B* **59**, 1758 (1999).

16. J. P. Perdew and Y. Wang, *Phys. Rev. B* **45**, 13 244 (1992).
17. 16.17. Z. J. Chen, H. Y. Xiao, X. T. Zu and F. Gao, *J. Appl. Phys.* **104**, 093702 (2008).
18. J. A. L. Rabone and N. H. de Leeuw, *J. Comput. Chem*. **27**, 253 (2006).
19. B.W.H. Van Beest, G.J. Kramer and R.A. Van Santen, *Phys. Rev. Lett.* **64**, 1955 (1990).
20. J. D. Gale and A. L. Rohl, *Mol. Simul*. **29**, 291 (2003).
21. P. Mogilevsky, E. B. Zaretsky, T. A. Parthasarathy and F. Meisenkothen, *Phys. Chem. Minerals*. **33**, 691 (2006).
22. D. F. Shanno, *Math. Comput.*, **24**, 647 (1970).
23. I. T. Todorov, W. Smith, K. Trachenko and M. T. Dove, J. Mater. Chem. **16**, 1911 (2006).
24. H. J. C. Berendsen, J. P. M. Postma, W. F. van Gunsteren, A. DiNola and J. R. Haak. *J. Chem. Phys*., **81(8)**, 3684 (1984).
25. R. Devanathan, L. Van Brutzel, A. Chartier, C. Guéneau, A. E. Mattsson, V. Tikare, T. Bartel, T. Besmann, M. Stan and P. Van Uffelen, *Energy. Environ. Sci*. (2010) DOI: 10.1039/C0EE00028K.

ACKNOWLEDGMENTS

This work was supported by the U. S. Department of Energy's Nuclear Energy Advanced Modeling and Simulation (NEAMS) Program at the Pacific Northwest National Laboratory, which is operated by Battelle for the U. S. Department of Energy under Contract No. DE-AC05-76RL01830. The authors acknowledge valuable discussions with Haiyan Xiao (University of Tennessee), Peter Schultz and Veena Tikare (Sandia National Laboratories) and Prashant Selvaratnam and Ian Farnan (University of Cambridge).